Available online at www.sciencedirect.com
ScienceDirect
Intermetallics 15 (2007) 706–710
Intermetallics
www.elsevier.com/locate/intermet

Study of serrated flow and plastic deformation in metallic glasses through instrumented indentation

W.H. Li [a,c], B.C. Wei [a,*], T.H. Zhang [b], D.M. Xing [b], L.C. Zhang [a], Y.R. Wang [a]

[a] National Microgravity Laboratory, Institute of Mechanics, Chinese Academy of Sciences, Beijing 100080, PR China
[b] State Key Laboratory of Nonlinear Mechanics (LNM), Institute of Mechanics, Chinese Academy of Sciences, Beijing 100080, PR China
[c] School of Materials Science and Engineering, Anhui University of Technology, Maanshan 243002, PR China
Available online 13 November 2006

Abstract

The plastic deformation behavior and serrated flow in seven bulk metallic glass (BMG) systems were investigated through instrumented indentation. These materials include $Ce_{65}Al_{10}Ni_{10}Cu_{10}Nb_5$, $Mg_{65}Cu_{25}Gd_{10}$, $Pd_{43}Ni_{10}Cu_{27}P_{20}$, $Cu_{60}Zr_{20}Hf_{10}Ti_{10}$, $Pt_{57.5}Cu_{14.7}Ni_{5.3}P_{22.5}$, $Ni_{60}Nb_{37}Sn_3$ and $Fe_{43}Cr_{16}Mo_{16}C_{15}B_{10}$ BMGs, which show a glass transition temperature (T_g) ranging from 360 to 908 K at a heating rate of 0.33 K/s. Remarkable difference in deformation behavior was found among these BMGs in the load–depth curves during nanoindentation. Prominent serrations are observed in Mg-, Pt- and Pd-based BMGs with medium T_g during the loading process, whereas no distinct serrated flow was found in Ce-, Ni- and Fe-based BMGs with quite low or high T_g. The subsurface plastic deformation regions after indentation were investigated using depth-sensing microindentation to characterize the shear band feature developed in various BMG systems. The size of the shear band upset is found to be larger in the alloys with lower T_g. The effect of T_g on the operation of shear bands and the serrated flow behavior in various BMG systems were discussed.

Keywords: B. Glasses, metallic; B. Plastic deformation mechanisms; B. Mechanical properties at ambient temperature

1. Introduction

Although bulk metallic glasses (BMGs) have shown potential as structural materials due to their high strength, high hardness, good wear resistance, excellent elasticity and easily forming in viscous state, applications are currently limited by the lack of any significant plastic deformation at room temperature. Understanding the micromechanisms of plastic deformation and developing the constitutive relationships for BMGs are active areas of research [1–7]. Recently, nanoindentation has been proposed as a key method for the study of localized deformation by shear banding in BMGs [8–15]. A lot of work has been focused on the loading rate effect on serrated flow and structural change in shear bands. Schuh and Nieh [5,9] identified a rate dependence on the nanoindentation response in metallic glasses, wherein slow indentations promote a serrated flow, while more rapid indentations can partially or even completely suppress the appearance of such serrations. They constituted a new high-rate regime of homogeneous flow on the deformation map of metallic glasses using elevated temperature nanoindentation. The data from $Pd_{40}Ni_{40}P_{20}$ and $Mg_{65}Cu_{25}Gd_{10}$ BMGs superpose quite well into a single deformation map, when the temperature is scaled to the glass transition temperature (T_g) [14]. This suggests that there is a possible general deformation map for metallic glasses with respect to T_g and strain rate. In this work, we studied the deformation behavior in seven BMG systems with T_g ranging from 360 to 908 K through nanoindentation at different loading rates. Moreover, the shear band pattern underneath the indents after indentation was characterized for further understanding of the deformation mechanism in various BMG systems.

* Corresponding author. Tel.: +86 10 62614945; fax: +86 10 62615524.
E-mail address: weibc@imech.ac.cn (B.C. Wei).

0966-9795/$ - see front matter © 2006 Elsevier Ltd. All rights reserved.
doi:10.1016/j.intermet.2006.10.010

2. Experimental

Seven alloys with the nominal chemical composition of $Ce_{65}Al_{10}Ni_{10}Cu_{10}Nb_5$, $Mg_{65}Cu_{25}Gd_{10}$, $Pt_{57.5}Cu_{14.7}Ni_{5.3}P_{22.5}$, $Pd_{43}Ni_{10}Cu_{27}P_{20}$, $Cu_{60}Zr_{20}Hf_{10}Ti_{10}$, $Ni_{60}Nb_{37}Sn_3$ and $Fe_{43}Cr_{16}Mo_{16}C_{15}B_{10}$, respectively, were studied. Cylindrical rods with 3 mm diameter of Ce-, Pt-, Pd-, Ni- and Fe-based BMGs were prepared by melting pure metals in an argon atmosphere and then chill-casting into a copper mould. The $Mg_{65}Cu_{25}Gd_{10}$ alloy was processed by melting pure Mg with Cu–Gd intermediate alloy and then chill-casting into a copper mould with the inner diameter of 5 mm. Thermal analysis was performed with a Perkin–Elmer DSC-7 differential scanning calorimeter under argon atmosphere. A constant heating rate of 0.33 K/s was employed. The specimens for nanoindentation measurements were mechanically polished to a mirror finish and tested in a MTS Nano Indenter® XP with a Berkovich diamond tip. Fused silica was used as a reference sample for the initial tip calibration procedure. The indentations were performed in load-control mode to a depth limit of 1 μm using loading rates from 0.075 to 5 mN/s. The thermal drift of the instrument was maintained below 0.05 nm/s. At least six indentations were made for each test. All tests were carried out at 296 K (room temperature). The study of subsurface deformation morphology was carried out through a depth-sensing microindentation using bonded interface technique. The detailed experimental process was provided in Refs. [15,16]. The observations of the upper surface and subsurface of the indents after indentation were performed by a JSM-6460 scanning electron microscope (SEM) and a Neophot-21 optical microscope.

3. Results and discussion

The glass transition temperatures of the present seven BMGs, $Ce_{65}Al_{10}Ni_{10}Cu_{10}Nb_5$, $Mg_{65}Cu_{25}Gd_{10}$, $Pt_{57.5}Cu_{14.7}Ni_{5.3}P_{22.5}$, $Pd_{43}Ni_{10}Cu_{27}P_{20}$, $Cu_{60}Zr_{20}Hf_{10}Ti_{10}$, $Ni_{60}Nb_{37}Sn_3$ and $Fe_{43}Cr_{16}Mo_{16}C_{15}B_{10}$, were determined by DSC measurements at a heating rate of 0.33 K/s. The results are listed in Table 1. The Ce-based BMG exhibits the lowest T_g of 360 K, while the Fe-based BMG shows the highest value of 908 K among these alloys. The nanoindentation measurements on each specimen were conducted at room temperature. The ratio of T/T_g (T: room temperature) of these alloys ranges from 0.33 to 0.82 (Table 1). The hardness (H) and modulus of elasticity (E) values of each alloy are derived using Oliver–Pharr method, and the results are listed also in Table 1. The Fe-based BMG shows the highest hardness and modulus of 17.9 GPa and 282.4 GPa, respectively, while the Ce-based BMG shows the lowest hardness and modulus of 1.7 GPa and 40.1 GPa, respectively.

Table 1
Mechanical parameters and glass transition temperature T_g of seven BMGs

Alloys	H (GPa)	E (GPa)	T_g (K)	T/T_g
$Ce_{65}Al_{10}Ni_{10}Cu_{10}Nb_5$	1.74	40.1	360	0.822
$Mg_{65}Cu_{25}Gd_{10}$	2.7	65.4	409	0.724
$Pt_{57.5}Cu_{14.7}Ni_{5.3}P_{22.5}$	6.0	129	500	0.592
$Pd_{43}Ni_{10}Cu_{27}P_{20}$	7.3	122.3	566	0.523
$Cu_{60}Zr_{20}Hf_{10}Ti_{10}$	8.8	131.1	722	0.410
$Ni_{60}Nb_{37}Sn_3$	13.3	217.2	889	0.333
$Fe_{43}Cr_{16}Mo_{16}C_{15}B_{10}$	17.9	282.4	908	0.326

T: room temperature.

Typical load–displacement (P–h) curves for nanoindentations on each of the seven amorphous alloys are presented in Fig. 1a, where the BMGs are indented to the depth of 1000 nm at a constant loading rate of 1 mN/s. At this loading rate, serrated flow in the loading parts of the P–h curves is observed in Pd-, Mg- and Pt-based BMGs with the T/T_g value from 0.52 to 0.72. While no distinct serrations can be found in Ce-, Cu-, Ni-, and Fe-based BMGs with quite high or low T_g. Serrated flow phenomenon is manifested as a stepped load–displacement curve punctuated by discrete bursts of plasticity during nanoindentation. It has been proposed that each serration corresponds to the activation of individual shear bands [5,9]. The serrated flow feature in the present Pd- and Mg-based BMGs agrees well with that of similar BMGs at comparable indentation rates [5,9,10,12].

The previous study on the deformation behavior during nanoindentation has proved that the serrated flow in Pd-, Zr- and

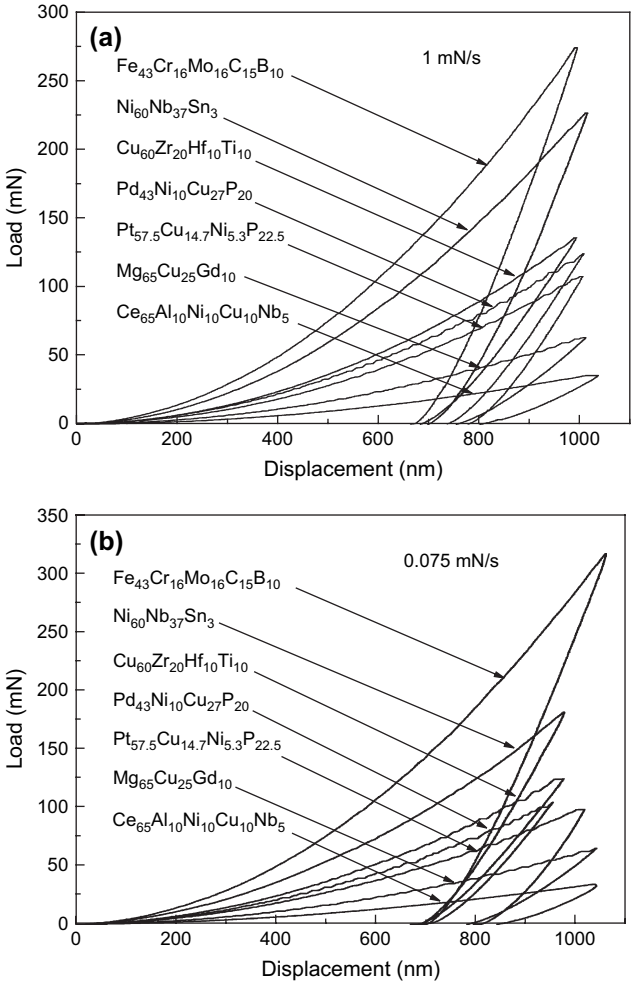

Fig. 1. Typical load–displacement (P–h) curves during nanoindentation at the loading rate of 1 mN/s (a) and 0.075 mN/s (b) for seven BMGs.

Mg-based BMGs depends strongly on the loading rate, wherein a more pronounced serrations appear at low loading rates. Here, loading rates from 0.075 to 5 mN/s were employed for a systemic study of the deformation behavior in these BMGs. The $P-h$ curves during nanoindentation at a low loading rate of 0.075 mN/s are shown in Fig. 1b. It can be seen that Pd-, Mg- and Pt-based BMGs exhibit a more pronounced serrated flow than that at 1 mN/s (Fig. 1a), and the Cu-based BMG ($T/T_g = 0.41$) also exhibits a moderate serrated flow at this low loading rate. In contrast, the Ce-, Ni- and Fe-based BMGs still do not exhibit distinct serrations during the loading processes. It is shown from Fig. 1a and b that serrations are more prominent at low loading rates for Pd-, Pt-, Mg-, and Cu-based BMGs. This tendency is consistent with that in Zr-, Pd-, Mg- and La-based BMGs during nanoindentation [5,9,10,12].

Depending on the plastic deformation feature of the above BMGs during nanoindentation, we plot a deformation map concerning the strain rate and T_g (scaled by T/T_g). Fig. 2 illustrates the deformation map based on the data of nine BMG alloys, where the data of $La_{55}Al_{25}Cu_{10}Ni_5Co_5$ and $Zr_{52.5}Al_{10}Ni_{10}Cu_{15}Be_{12.5}$ are taken from Refs. [10,15]. It can be found in Fig. 2 that, the most prominent serrated flow appears at low strain rates and only in the T/T_g range from about 0.5 to 0.75. While, a moderate serrated flow takes place at the low strain rates in the T/T_g range from 0.4 to 0.5. For the quite high T/T_g (>0.8) or quite low T/T_g (<0.35) range, there is no serration at all strain rates. The heavy serration region in this map agrees with the results of Schuh et al., which exhibit a heavy serration region in the T/T_g ranges from 0.65 to 0.82 at low strain rates, based on the elevated nanoindentation results in Mg- and Pd-based BMGs [14].

For further understanding of the deformation behavior of the BMGs related to different T_g values, the plastic deformation

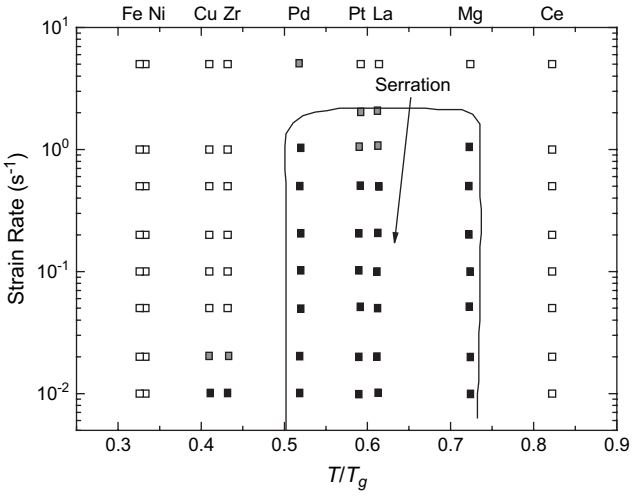

Fig. 2. The plastic deformation map concerning T/T_g values and indentation strain rate of nine BMGs. The symbols are shaded according to the degree of flow serration: prominent serration (black), moderate serration (gray) and light or no serration (white).

region around the indents after indentation was studied. Typical surface morphologies of indents for the six BMGs after indentation at the loading rate of 1.0 mN/s are shown in Fig. 3. A number of incomplete circular patterns of shear bands were observed in the pile up area around the indents for Mg-, Pt-, Pd-, Cu-, Ni- and Fe-based BMGs. However, the number of shear bands around the indents is relatively small in the Fe- and Ni-based BMGs, which do not show distinct serrated flow during nanoindentation. Few shear bands were also observed in the Ce-based BMG after indentation [17]. The shear bands around the indents indicate that the plastic deformation of these BMGs

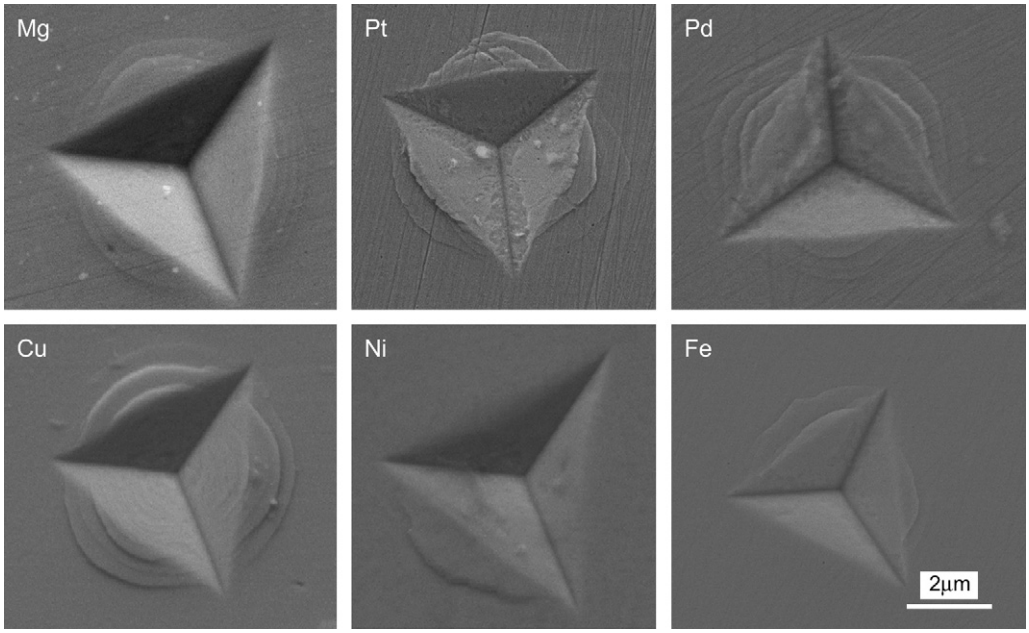

Fig. 3. SEM images of the morphology around the indents' nanoindentation at the loading rate of 1 mN/s for six BMGs.

is highly localized irrespective of whether there is serrated flow during indentation or not.

To clearly characterize the deformation mechanism in the BMGs with a wide range of T_g, the underneath deformation region of typical alloys was investigated through depth-sensing microindentation using bonded interface technique. Fig. 4 exhibits the shear pattern underneath the indents after microindentation for Fe-, Mg- and Ce-based BMGs with similar fracture toughness. Many semi-circular and radial shear bands are observed in the plastic deformation region of all the three BMGs. It is interesting to find that the Fe-based BMG with high T_g shows the finest shear band upset, while the Ce-based BMG with the lowest T_g exhibits the largest shear band upset. The Mg-based BMG along with Zr-based BMGs [15] exhibits a moderate shear band size. This suggests that the size of shear band increases with decreasing T_g.

To clarify the shear band and serrated flow features in the BMGs with different T_g, one should consider the nucleation process of shear bands. Argon [17] and later Falk [18,19] proposed the term ''shear transformation zone'' (STZ) to describe the local shear events. According to the STZ model the amorphous material can be divided into two volumes: one is the STZ, which will become the nucleus of a shear band; the other is the glassy matrix. Under an applied stress a small embryonic shear band near the STZ will undergo distortion and deformation. The ratio of the strain rate in shear band $(\dot{\gamma}_n)$ to that of the surrounding matrix $(\dot{\gamma})$ is given as:

$$\dot{\Gamma}_0 = \frac{\dot{\gamma}_n}{\dot{\gamma}} = \exp\left(\frac{\varphi \Delta F_0}{kT}\right) \quad (1)$$

where φ is the fraction of the transformation strain energy stored in each STZ-sized volume, and is of the order ~ 0.08, ΔF_0 is the free energy required to operate the STZ, k is the Boltzmann constant and T is the temperature. Eq. (1) indicates that the nucleation of shear bands begins with a very localized region in the glass, which deforms more quickly than the rest. A trend can be seen here that $\dot{\Gamma}_0$ deceases rapidly as the homologous temperature (T/T_g) is increased. This tendency is intuitive, as high homologous temperature (~ 1) promotes rapid viscous flow of the matrix, which can become nearly of the same order as that in the shear band near the glass transition. The serrated flow during plastic deformation of metallic glasses is caused by the sudden release of elastic energy around shear bands due to their rapid propagation. For the present alloys with high T/T_g values (>0.8), the shear rate in shear bands decreases relative to that of the surrounding matrix. This consequently weakens the sudden release of the elastic energy, and leads to the disappearance of serrated flow during nanoindentation. In contrast, for the alloys with quite low T/T_g values (<0.35), the strain rate in shear bands is extremely high. The operation of shear bands and the rigid movement of the matrix may exceed the resolving ability of the instrument, thereby serrated flow cannot be found in the $P-h$ curves during nanoindentation either.

The larger shear bands in the alloy with higher T/T_g values are related to the shear band dynamics. According to Spaepen [20], free volume is created by an applied shear stress and annihilated by a series of atomic jumps. The latter item is a thermally activated process related to the temperature. The alloys with low T/T_g values have a lower atomic mobility, as room temperature is far below the glass transition temperature. Therefore, the volume of materials which are involved in the nucleation process of shear bands in the alloys with lower T/T_g values is smaller than that in the alloys with higher T/T_g. That is, low T/T_g values promote small shear bands, more finely spaced in the spatial scale.

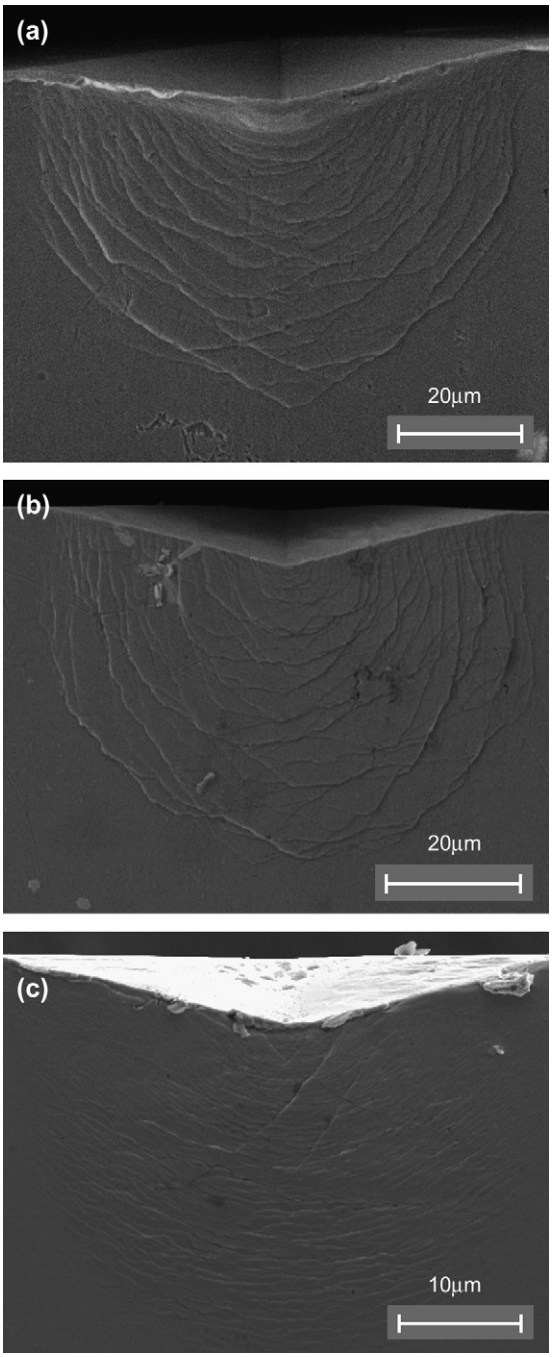

Fig. 4. SEM images of the deformation region underneath a Vickers indenter for (a) $Ce_{65}Al_{10}Ni_{10}Cu_{10}Nb_5$; (b) $Mg_{65}Cu_{25}Gd_{10}$; (c) $Fe_{43}Cr_{16}Mo_{16}C_{15}B_{10}$ bulk metallic glasses.

4. Summary

Serrated flow feature in $Ce_{65}Al_{10}Ni_{10}Cu_{10}Nb_5$, $Mg_{65}Cu_{25}Gd_{10}$, $Pt_{57.5}Cu_{14.7}Ni_{5.3}P_{22.5}$, $Pd_{43}Ni_{10}Cu_{27}P_{20}$, $Cu_{60}Zr_{20}Hf_{10}Ti_{10}$, $Ni_{60}Nb_{37}Sn_3$ and $Fe_{43}Cr_{16}Mo_{16}C_{15}B_{10}$ bulk metallic glasses are studied using instrumented indentation. Prominent serrated flow is only observed at low loading rates during nanoindentation for the alloys with moderate glass transition temperature. Highly developed shear band pattern is observed around the indents in all seven alloys after indentation measurements, where larger shear bands form in the alloy with relatively low glass transition temperature.

Acknowledgements

The authors would like to acknowledge the financial support provided by National Nature Science Foundation of China (Grant Nos. 50571109, 10572142 and 10432050) and the Knowledge Innovation Program of Chinese Academy of Sciences.

References

[1] Hays CC, Kim CP, Johnson WL. Phys Rev Lett 2000;84:2901.
[2] He G, Eckert J, Löser W, Hagiwara M. Acta Mater 2003;52:3035.
[3] Flores KM, Dauskardt RH. Intermetallics 2004;12:1025.
[4] Ma H, Xu J, Ma E. Appl Phys Lett 2003;83:2793.
[5] Schuh CA, Nieh TG. J Mater Res 2004;19:46.
[6] Inoue A. Acta Mater 2000;48:279.
[7] Li J, Spaepen F, Hufnagel TC. Philos Mag A 2002;82:2623.
[8] Kim JJ, Choi Y, Surech S, Argon AS. Science 2002;295:654.
[9] Schuh CA, Nieh TG. Acta Mater 2003;51:87.
[10] Nieh TG, Schuh CA, Wadsworth J, Li Y. Intermetallics 2002;10:1177.
[11] Jiang WH, Atzmon M. J Mater Res 2003;18:755.
[12] Greer AL, Walker IT. Mater Sci Forum 2002;77:386.
[13] Wei BC, Zhang TH, Li WH, Sun YF, Yu Y, Wang YR. Intermetallics 2004;12:1239.
[14] Schuh CA, Lund AC, Nieh TG. Acta Mater 2004;52:5879.
[15] Li WH, Zhang TH, Xing DM, Wei BC, Wang YR, Dong YD. J Mater Res 2005;21:75.
[16] Xing DM, Zhang TH, Li WH, Wei BC. J Alloys Compd, in press.
[17] Argon AS. Acta Metall 1979;27:47.
[18] Falk ML. Phys Rev B 1999;60:7062.
[19] Falk ML. Phys Rev E 1998;57:7192.
[20] Spaepen F. Acta Metall 1977;25:407.